Available online at www.sciencedirect.com
ScienceDirect
International Journal of Mass Spectrometry 263 (2007) 59–65
International Journal of Mass Spectrometry
www.elsevier.com/locate/ijms

Ion dynamics in non-perfect quadrupole traps

Xiao-Guang Wu *

Varian, Inc., 2700 Mitchell Drive, Walnut Creek, CA 94598, USA

Received 13 October 2006; received in revised form 20 December 2006; accepted 21 December 2006
Available online 8 January 2007

Abstract

Ion dynamics in non-perfect quadrupole traps differ from those in a pure quadrupole field. We obtain an analytic expression for a quadrupole field superimposed with weak, higher-order multipole fields. Single ion dynamics in such trapping fields close to the instability point are investigated. We show that for an in-phase octopole field, oscillating envelopes of the axial displacement grow exponentially with the parameter deviation; whereas for an out-of-phase octopole field the growth of the oscillating envelopes follows a square-root law. A hard-sphere scattering model is assumed to incorporate collisions with buffer-gas molecules. The collision frequency and cross-section are defined. A simulation algorithm for many-ion dynamics is developed based on the Verlet algorithm and Monte Carlo techniques. We show how a weak octopole field affects the mass resolution in a significant way.

Keywords: Multipole expansion; Non-linear dynamics; Bifurcation; Molecular dynamics; Hard-sphere scattering

1. Introduction

Ions can be trapped and held at a well-localized position using a number of different schemes. The most popular schemes, first introduced by Paul and Steinwedel in 1953 [1] are based on the formation of a quadrupole electric field using a set of three electrodes. Ideally, the surfaces of the electrodes are hyperboloids of revolution, following the equipotential surfaces of an ideal quadrupole potential. In reality, simpler shapes are often used when the resulting small deviations from a pure quadrupole potential can be tolerated.

The Paul trap is, theoretically, an ion trap with *perfect* quadrupole geometry. In this case the field is uncoupled in the three coordinate directions so the forces in each direction can be determined separately, and the ion trajectories can be described by the Mathieu equation [2–4]:

$$\frac{\mathrm{d}^2u}{\mathrm{d}\tau^2} + [a_u - 2q_u\cos(2\tau)]u = 0; \quad u = x, y, \text{or } z \tag{1}$$

In Eq. (1) τ is the dimensionless time defined as $\tau = \Omega t/2$ with Ω the ac frequency, also referred as rf (radio frequency) in mass spectrometry; a_u and q_u are, respectively, dimensionless dc and ac amplitudes defined as

$$a_u = \chi_u U, \quad q_u = \chi_u V,$$

$$\text{with } \chi_u = \frac{I_u}{(m/e)(r_0^2 + 2z_0^2)\Omega^2}, \quad I_u = \begin{cases} -2 & \text{for } u = x, y \\ 4 & \text{for } u = z \end{cases}$$

m/e is the ion's mass-to-charge ratio, r_0 and z_0 geometry parameters (see Fig. 1), and U and V are, respectively, the dc and rf voltage at the ring electrode with the end-caps grounded. According to the *Floquet theorem* [5,6] stable solutions of the Mathieu equation, corresponding to stable ion trajectories in a pure quadrupole field, are known to have general form of a Fourier–Taylor series:

$$u(\tau) = \exp(\mathrm{i}\beta_u\tau)\sum_{n=0}^{\infty} A_{2n,u}\exp(2\mathrm{i}n\tau) + \text{c.c.} \tag{2}$$

Here, β_u is the Floquet frequency depending on the dc and rf amplitudes a_u and q_u, its value is usually altered by varying the rf amplitude; and c.c. stands for complex conjugate. Solutions of the Mathieu equation will grow unbounded when the resonance conditions are met; *i.e.*, $\beta_u = 0, 1, 2, \ldots$ In this paper we only study the resonance instability with $\beta_z = 1$, corresponding to one half of the rf frequency. When $\beta_z > 1$ ions are ejected from the ion trap and are detected.

* Current address: Revionics, Inc., 9785 Goethe Road, Sacramento, CA 95827-3559, USA.
E-mail address: cwu@revionics.com.

1387-3806/$ – see front matter © 2007 Elsevier B.V. All rights reserved.
doi:10.1016/j.ijms.2006.12.007

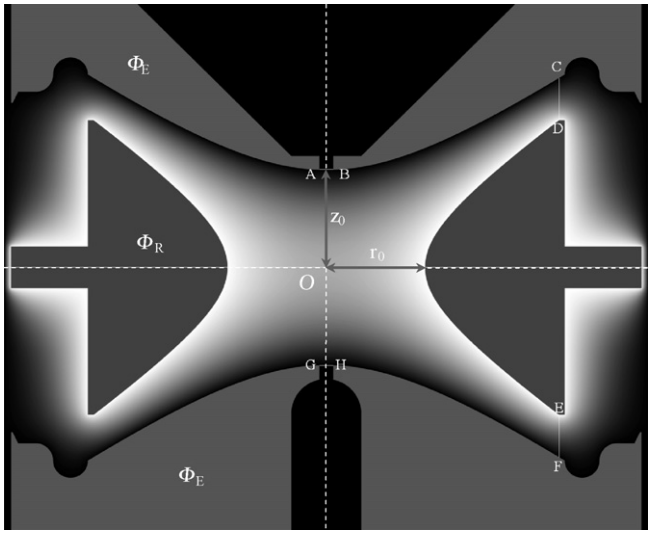

Fig. 1. Cross-sectional view of a typical 3D "truncated" ion trap with $r_0 = z_0 = 7.07$ mm. The potential $\Phi(r, z)$ obtained with FDM is plotted as grey scale from white for $\Phi = \Phi_R$ to black for $\Phi = \Phi_E$. The vertical dash line is the axis of rotational symmetry. The expansion coefficients C_n for this geometry are shown in the fourth column of Table 1.

Designers of new ion traps have purposely created weak superimposed multipole fields to improve mass resolution, scan speed and storage stability; a well known example is the Finnigan MAT ion trap [7], whose end-cap electrodes are slightly stretched from the center of the device. Even if the electrodes are shaped precisely to generate pure quadrupole fields, weak multipoles are introduced by the edges of the electrodes, and when there are small holes on end-caps for ion injection and ejection. Therefore, it is impossible to neglect completely the high-order multipoles in the trapping field for stability analysis for ion trajectories.

In this study we write the trapping-field potential in terms of multipoles; *i.e.*,

$$\phi(\mathbf{r}, t) = \sum_n C_n \cos(\Omega t)\phi_n(\mathbf{r}) \tag{3}$$

where $\phi_n(\mathbf{r})$ is the $2n$-pole potential, and Ω is the rf frequency. The expansion coefficients C_n in Eq. (3) are determined using a hybrid LS-FD method (least square-finite difference method). Examples of expansion coefficients are presented in Table 1.

The dynamics of ion–buffer-gas collision is also modeled in this study. We derive the collision frequency and the collision cross-section, and formulate the probabilistic update rules for the collision dynamics. The collision cross-section is estimated using the Gaussian 03 program package that optimizes the ion's geometry by minimizing its bonding energies.

In Section 3 we present a generalized MD (molecular dynamics) algorithm for ionic motion in a trapping field described by Eq. (3). Not only is the trapping filed taken into account, but also the ion–ion interaction and ion–buffer-gas collisions are integrated in our MD model. Finally, in Section 4 we summarize and discuss results obtained in this paper.

Table 1
Expansion coefficients for the truncated ion trap shown in Fig. 1 ($r_0 = z_0 = 7.07$ mm) with (C_n^H) and without (C_n^T) holes on the end-cap electrodes for $\Delta\Phi = \Phi_R - \Phi_E = 1$

n	C_n^T	C_n^T/C_2 (%)	C_n^H	C_n^H/C_2 (%)
0	0.66360965	99.541	0.66413665	99.620
2	−0.66376241	99.564	−0.66238876	99.358
4	−0.00341752	00.513	−0.00293904	00.441
6	−0.00055028	00.083	−0.00037950	00.057
8	−0.00037885	00.057	−0.00035341	00.053
10	−0.00004673	00.007	−0.00004250	00.006
12	−0.00000739	00.001	−0.00000712	00.001
14	−0.00000055	00.000	−0.00000053	00.000

$C_2 = -2/3$ is the quadrupole coefficient of the pure quadrupole trap with the same r_0 and z_0.

2. Single-ion dynamics

For a single ion with mass-to-charge ratio m/e in a trapping field the equation of motion can be written as, according to classical electrodynamics [8], $\ddot{\mathbf{r}} = -(e/m)\nabla\phi(\mathbf{r}, t)$; or, more explicitly [2–4]:

$$\ddot{\mathbf{r}}(t) = -\frac{e}{m}[U - V\cos(\Omega t)]\sum_n C_n \nabla\phi_n(\mathbf{r}(t)) \tag{4}$$

Here, U and V are defined below Eq. (1), $\phi_n = (\rho/r_0)^n P_n(\cos\theta)$ is the $2n$-pole potential in cylindrical coordinate system with P_n the Legendre polynomial of order n; the C_n can be determined by a hybrid LS-FD method similar to that of Wang and Franzen [9] who evaluated the potential value along the "truncating line" using a numerical method such that all the potential values at a closed boundary are known. The only difference is that we solve the Laplace equation directly with FDM to get the potential values at open areas such as lines $\overline{AB}$, $\overline{CD}$, $\overline{EF}$, and $\overline{GH}$ in Fig. 1. The Laplace equation was solved on the entire space shown in Fig. 1. We found that electrodes outside the trap also influence the potential within the trap, same as Ding reported in their calculations [10]. The electrode's voltages (potentials) are defined as $\Phi_E = 0$ and $\Phi_R = 1$ V. Once all the potential values on a closed boundary are known, the expansion coefficients C_n can be determined readily using the LSM [11]. Examples of the C_n are listed in Table 1.

2.1. The octopole field

As opposed to Eq. (1) where ionic motion is independent in the three spatial directions, the ionic motion described by Eq. (4) is slightly different due to high-order multipoles in the potential function. For a truncated ion trap, such as the one shown in Fig. 1, the leading higher-order term is the octopole potential:

$$\phi_4(r, z) = \left(\frac{\rho}{r_0}\right)^4 P_4(\cos\theta) = \frac{8z^4 - 24z^2r^2 + 3r^4}{8r_0^4} \tag{5}$$

The z^2r^2 term in Eq. (5) couples the axial and the radial motions. In this case the equation of motion along the z-axis, accurate to

the octopole term, is

$$z_{\tau\tau} + [\tilde{a}_z(r,z) - 2\tilde{q}_z(r,z)]\cos(2\tau)z = 0 \tag{6}$$

where $\tilde{a}_z(r,z) = a_z[1+\varepsilon(z^2 - 3r^2/2)]$ and $\tilde{q}_z(r,z) = q_z[1+\varepsilon(z^2-3r^2/2)]$ are, respectively, the effective dc and rf amplitudes in the presence of weak octopole field, $z_{\tau\tau}$ is short for $d^2z/d\tau^2$, and ε is a small parameter proportional to the octopole expansion coefficient C_4 and can be expressed explicitly as

$$\varepsilon = \frac{4C_4}{r_0^2} \tag{7}$$

Further simplicity can be made by using an approach adopted in Ref. [12]; Eq. (6) then reduces to

$$z_{\tau\tau} + [a_z - 2q_z\cos(2\tau)]F(z) = 0 \tag{8}$$

with $F(z) = (1 - \varepsilon 3\bar{r}^2/2)z + \varepsilon z^3$. In $F(z)$ $\bar{r}$ is the radial displacement averaged over one secular cycle. Here, again, the axial motion is decoupled from the radial motion when the coupling is insignificant ($\sim\varepsilon$). For small values of $\bar{r}$ (*i.e.*, when ions are close to the center of the trap) $F(z)$ can be simplified further

$$F(z) = z + \varepsilon z^3 \tag{9}$$

since the dropped term in the linear coefficient is of order ε. We will use Eq. (9) as the non-linear field for further analyses.

2.2. The non-linear Mathieu equation, bifurcations, and ion ejection speed

Eq. (8) can be written as a non-linear Mathieu equation of the general form

$$z_{\tau\tau} + [\alpha^2 + p(\tau)]F(z) = 0 \tag{10}$$

where $p(\tau)$ is time-periodic and $F(z)$ is a non-linear function of z. Parametric excitation in second order differential equations with periodic coefficients such as Eq. (10) has been studied extensively since last decade [13–17].

A bifurcation is a qualitative change in the dynamics of a system as a control (excitation) parameter exceeds a critical value, such as $\beta_z = 1$. The control parameters in the non-linear Mathieu equation are the tuning parameter $\sigma = \alpha^2 - n^2$ (similar to a_z), and the Fourier expansion of $p(t)$ containing non-zero terms $a_{2n}\,e^{2in\pi}$ and $a_{-2n}\,e^{-2in\pi}$ (similar to q_z). Eq. (10) can be rewritten in a complex *normal form* (see, for instance, Refs. [18,19] for normalization of time-dependent vector fields):

$$\xi_\tau = in\xi + \frac{i\sigma}{2n}\xi + \frac{ia_{2n}}{2n}e^{2int}\xi^* + \cdots + g\xi|\xi|^2 + O(\varepsilon) \tag{11}$$

where $\xi = nz - i\,dz/d\tau$ and $g = 3c_3/4$. The normal form (11) can be made *autonomous* through the transformation $\xi = \sqrt{\varepsilon}\,e^{in\tau}\eta$:

$$\frac{d\eta}{dT} = i\sigma\eta + ia_{2n}\eta^* + \sqrt{\varepsilon}K + ig\eta|\eta|^2 + O(\varepsilon) \tag{12}$$

where $T = \varepsilon\tau$, and the explicit expression for K is lengthy and can be found in Ref. [14]. When $p(\tau) = 2a_2\cos 2\tau$ [cf. Eq. (8)] we have $K = 0$ (see Ref. [14] for proof), Eq. (12) thus reduces to

$$\frac{d\eta}{dT} = i\sigma\eta + ia_{2n}\eta^* + ig\eta|\eta|^2 + O(\varepsilon) \tag{13}$$

It is not difficult to show that, for sufficiently large radius R in the Re(η)–Im(η) *plane*, the disc $|\eta| < R$ is *invariant* under the *flow* (13), and that the only *attractors* in this region are *fixed points*. For simplicity we only consider the case where $n = 2$ that corresponds to $P(\tau) = 2a_2\cos(2\tau)$. When $a_{2n} + \sigma > 0$ and $g < 0$ (*i.e.*, when $\beta_z > 1$ and when the octopole filed is negative or out of phase with the quadrupole field) the bifurcation is *supercritical* (also called *pitchfork bifurcation*) and the non-trivial solution $|\eta|^2 = (a_{2n} + \sigma)/|g|$ is stable; whereas when $a_{2n} + \sigma > 0$ and $g > 0$ (*i.e.*, when $\beta_z > 1$ and when the octopole field is positive or in-phase with the quadrupole field) the bifurcation is *subcritical* and the non-trivial solution $|\eta|^2 = -(a_{2n} + \sigma)/g$ is unstable [20–23]. The supercritical and subcritical bifurcations are illustrated in Fig. 2(a and b) where the stable solutions are plotted with solid lines.

A stable non-trivial solution for negative octopole fields, emerging from the trivial solution $\eta = 0$ at the supercritical pitchfork bifurcation, grows with the square-root of the parameter

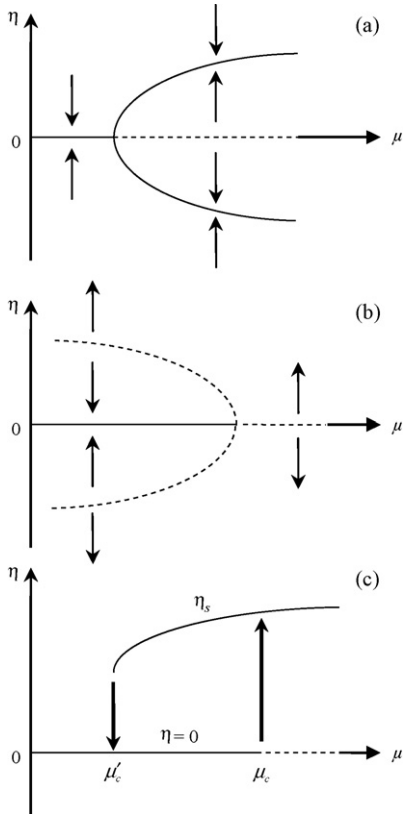

Fig. 2. Supercritical (a) and subcritical (b) bifurcations in the μ–η plane, arrows show the flow directions; (c) hysteresis loop (bistability). Here, η is proportional to the slowly varying envelope of the axial position of the ion, z, and μ is the bifurcation parameter depending on β_z and having the same sign as $(\beta_z - 1)$. The stable (unstable) solutions of Eq. (13) are plotted as solid (dashed) lines; μ_c is the value of the bifurcation parameter at which η bifurcates from the trivial solution $\eta = 0$. In (c) η will grow exponentially from 0 to η_s for $\mu > \mu_c$. The growing exponent can be calculated by solving the linear stablity matrix of Eq. (13) at $\mu = \mu_c$ for eigenvalues.

deviation $\sim\sqrt{(a_{2n}+\sigma)/|g|}$, this is exactly what is observed by the authors of Ref. [24] in their computer simulations for out-of-phase octopole fields. Recall that the trivial solution implies that $\xi = 0$, *i.e.*, $2z - \mathrm{i}\,\mathrm{d}z/\mathrm{d}\tau = 0$, or

$$z_t(\tau) = z_t(0)\,\mathrm{e}^{-2\mathrm{i}\tau} \tag{14}$$

This is a harmonic oscillation with the rf frequency. Note that $z_t(0)$ is an initial z-displacement that can take any value. As shown in Fig. 5A and B in Ref. [24], the growth of oscillating envelopes always follows the same square-root law, no matter what the value of initial amplitude is.

The unstable solution $|\eta|^2 = -(a_{2n}+\sigma)/g$ for $g > 0$ and $a_{2n}+\sigma > 0$ implies that there exists a stable, upper branch of the steady-state solution that can be obtained by using an additional term of order ε in Eq. (11). The canonical form of such an autonomous equation is

$$\frac{\mathrm{d}\eta}{\mathrm{d}T} = \mathrm{i}\mu\eta + \mathrm{i}g\eta|\eta|^2 - \mathrm{i}h\eta|\eta|^4 \tag{15}$$

where h is a real, positive parameter. The stable upper branch is

$$\eta_\mathrm{s} = \left[\frac{1}{2h}(-g + \sqrt{g^2 + 4h\mu})\right]^{1/2} \tag{16}$$

When $a_{2n}+\sigma > 0$ (*i.e.*, $\beta_z > 1$) η grows exponential from the trivial solution $\eta = 0$ [corresponding to $z(\tau) = z_t(\tau)$, cf. Eq. (14)] to the steady-state solution η_s (the upper branch). This is called *hysteresis loop* or *bistability* [18,19]. This scenario is illustrated in Fig. 2(c): the trivial solution loses its stability at critical point μ_c and jumps to the upper stable branch η_s; both the trivial solution and η_s are stable between the parameter range $\mu'_\mathrm{c} \le \mu \le \mu_\mathrm{c}$ (hence the term *bistability*), and η_s does not exist when $\mu < \mu'$. Fig. 5D in Ref. [24] shows such exponential growth (jump) of the $z(t)$ for positive octopole fields when the scan parameter exceeds the subcritical bifurcation point.

Note that the exponential growth of $z(t)$ beyond the bifurcation point corresponds to the ejection of ions from the ion trap. Therefore, when the octopole field is positive (negative) the ejection is exponential (a square-root law). This will directly affect the ejection speed and the mass resolution since slow ejections may cause adjacent mass peaks to overlap, resulting in a significantly reduced mass resolution. To illustrate how the sign of octopole field affects the ejection speed, we integrate Eq. (4) to get ion's axial displacement $z(t)$. When $z(t) > z_0$ the ion is considered as ejected (see Fig. 1). One can now define the ejection time t_e at which $z(t) = z_0$. Fig. 3 shows the ejection time t_e versus the octopole-to-quadrupole ratio, defined as $r_\mathrm{oq} = C_4/C_2$. As is clearly seen, when r_oq goes negative, the t_e increases significantly.

2.3. Ion–buffer-gas interaction

The presence of a buffer-gas such as helium or hydrogen,[1] at a pressure of approximately 10^{-3} Torr, significantly enhances the mass resolution, sensitivity and detection limit of an ion trap. The effect of collisions between trapped ions and the relatively slow moving and much less massive buffer-gas molecules causes viscous-like damping of ionic motion. This causes the ions' orbits to collapse closer to the center of the ion trap.

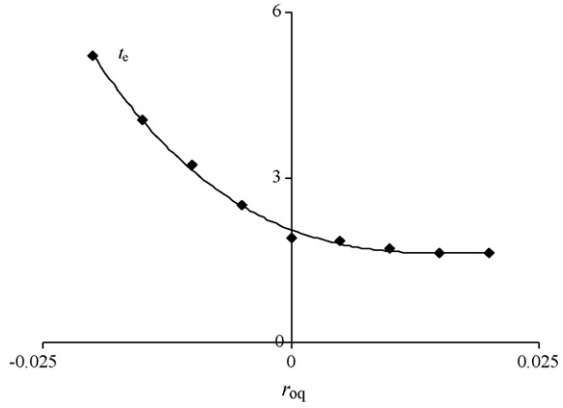

Fig. 3. The ejection time t_e vs. the octopole-to-quadrupole ratio $r_\mathrm{oq} = C_4/C_2$ (diamonds) for scan rate = 7.5 μs/Da, rf frequency $\Omega = 1$ MHz, and ion's mass to charge ratio $m/e = 185$. The t_e is plotted in units of μs. The smooth curve is a polynomial fit for t_e.

Let us consider the collision frequency between an ion with its velocity $\dot{\mathbf{r}}$ and buffer-gas molecules of mass m_b at temperature T [25,26]:

$$f = n_\mathrm{b}\left(\frac{m_\mathrm{b}}{2\pi k_\mathrm{B}T}\right)^{3/2}\int_0^{2\pi}\mathrm{d}\phi\int_0^{\pi}\sin\theta\,\mathrm{d}\theta \times\int_0^{\infty}|\dot{\mathbf{r}} - \mathbf{v}|\,\mathrm{e}^{-m_\mathrm{b}v^2/2k_\mathrm{B}T}\sigma v^2\,\mathrm{d}v \tag{17}$$

where n_b is the number density of the buffer-gas molecules, $\mathbf{v}$ its velocity ($v = |\mathbf{v}|$), k_B the Boltzmann constant, and σ the collision cross-section. We assume that both the trapped ion and the buffer-gas molecule can be modeled by *hard spheres*, *i.e.*, the interaction potential is infinity when the two particles are in contact and zero when separated. Eq. (17) can thus be simplified as [26]:

$$f = \dot{r}\sigma\frac{P}{k_\mathrm{B}T} = \dot{r}\pi\bar{D}^2\frac{P}{k_\mathrm{B}T}, \quad \bar{D} = \frac{d_i + d_\mathrm{b}}{2} \tag{18}$$

Here, $\bar{D}$ is the average diameter of the tapped ion and the buffer-gas molecule, P the pressure of buffer-gas, and T is the temperature. The collision frequency f measures how often collision events occur.

Furthermore, collisions between hard spheres are elastic; *i.e.*, both momentum and kinetic energy are conserved in the collision. This leads to a simple update law for an ion's post-collision momentum $\mathbf{p}'_i$:

$$\mathbf{p}'_i = 2m_i\mathbf{R}_z(-\phi_\mathrm{b})\mathbf{R}_y(-\theta_\mathrm{b})\mathbf{v}_\mathrm{CM} - \mathbf{p}_i \tag{19}$$

Here, $\mathbf{p}_i$ is the pre-collision momentum; $\mathbf{v}_\mathrm{CM}$ the pre-collision center-of-mass velocity of the ion and a buffer-gas molecule; ϕ_b and θ_b are, respectively, the random rotation and scattering angles; and $\mathbf{R}_y$ and $\mathbf{R}_z$ are the usual rotation matrices [27]. The type of elastic collision described above is called hard-sphere scattering. The detailed derivation of Eq. (19) is omitted here

[1] For the use of hydrogen as the buffer-gas, see Ref. [26].

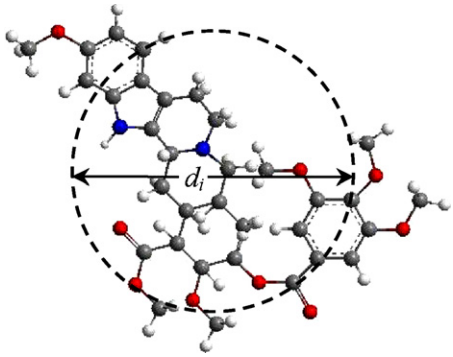

Fig. 4. Optimized molecular structure for *reserpine*. Its diameter is estimated to be, when assumed to be a sphere (dash line), $d_i = 11.5$ Å.

since this is a classical problem in mechanics and references are readily available.

2.4. Estimating ions' diameter

Our final challenge now is to calculate the diameter of the trapped ion, d_i, in Eq. (18), for the calculation of the collision frequency f. The geometric structures of molecules with medium to large size can be optimized with density functional methods at the B3LYP/6-31G* level [28–30]. Minimum energy path calculations will be performed to optimize the molecule's geometry and thus to estimate its diameter d_i. Fig. 4 shows an optimized 3D structure for a *reserpine* molecule. The calculations were carried out with the Gaussian 03 program package [31], and the ion's diameter was estimated to be, assuming the ion is a sphere, $d_i = 11.5$ Å. According to this value, the cross-section for hard-sphere collisions can be calculated as $\sigma = \pi \bar{D}^2 = \pi(d_i + d_b)^2/4 \approx 167.1$ Å^2. Here, we used the $d_b \approx 3.1$ Å [32] for helium as the buffer-gas. It should be noted that $\sigma \approx 167.1$ Å^2 is a very rough estimation since both ions and buffer-gas molecules are modeled as hard spheres; the experimentally measured collision cross-section for reserpine is about 1.7 times of our value [33].

3. Many-ion dynamics and simulations

3.1. Ion–ion interaction

There are two fundamental laws of electrostatics [8]. The first is Coulomb's law, which describes the force between two point charges; the second is the law of superposition, which extends Coulomb's law to more than two charges. Consider a system with N trapped ions. The total Coulomb force acting on the ith ion is, according to Coulomb's law, $\mathbf{F}_i^C = (e_i/4\pi\varepsilon_0)\sum_{j\neq i} e_j(\mathbf{r}_i - \mathbf{r}_j/|\mathbf{r}_i - \mathbf{r}_j|^3)$. Equation of motion (4) can then be written as

$$\ddot{\mathbf{r}}_i = -\frac{e_i}{m_i}\nabla\Phi(\mathbf{r}_i; t) + \frac{e_i}{4\pi\varepsilon_0 m_i}\sum_{j\neq i} e_j \frac{\mathbf{r}_i - \mathbf{r}_j}{|\mathbf{r}_i - \mathbf{r}_j|^3},$$

$$i, j = 1, 2, \ldots, N \tag{20}$$

The calculation of the Coulomb forces $\mathbf{F}_i^C$ is time-consuming and scales to N^2 where N is the total number of ions in the simulation. For large values of N the simulation will take an enormous amount of time. To overcome this slowness problem we adopt a space-charge model called *reduced-pressure model* [34]. In this approximation the space-charge effect is modeled by a reduced buffer-gas pressure such that the same space-charge distribution and the same mass spectra can be generated. With this model one can get linear scalability with N in simulating the Coulomb force effect, resulting in a much faster simulation speed.

3.2. Molecular dynamics

The equations of motion (20) describe a many-body dynamic system with $6N$ degrees of freedom. Due to the complicated nature of this system, there is no analytical solution to such equations of motion; they must be solved numerically. In this paper we adopt the *velocity Verlet* algorithm [35] to solve Eq. (20). The *Verlet* algorithm is among several computational methods that calculate the time-dependent behavior of a many-body molecular system by integrating its equations of motion with a finite step [36–38].

3.3. Probabilistic update rules

We adopt Monte Carlo techniques to simulate ion–buffer-gas collisions. More specifically, a hit-and-miss rule is applied to a computer-generated random number at equally spaced time interval to decide whether a random collision should occur at time t for ion i. The average collision per unit of time is designed to match f in Eq. (17), the collision frequency. When a collision occurs, we generate a random velocity for the buffer-gas molecule from the Maxwell–Boltzmann distribution for given pressure, temperature and mass. Once the random velocity is generated, we use Eq. (19) to update ion's post-collision momentum.

3.4. Mass spectra

The most important usage of an ion trap is the mass-selection instability scan. A mass spectrum can be constructed by counting numbers of ions exiting the trap at each rf cycle. By increasing linearly the rf field amplitude V_0 (linear scan) ions with different m/e values are ejected at different rf voltages. Fig. 5 shows the mass spectrum for reserpine ions with seven isotopes (mass to charge ratio m/e ranging from 607 to 613). The trapping-field amplitudes are $U = 0$, and $V(t) = 4150(1 + vt)$ V with $v = 6 \times 10^{-8}\Omega/\pi$ and $\Omega = 2\pi \times 10^6$ s^{-1}. As clearly seen in the figure, for the same scan rate v an additional octopole field can affect the mass resolution a great deal. For an in-phase octopole field all seven mass peaks are resolved, whereas for an out-of-phase octopole field the mass peaks overlap, showing only one broad peak approximately 8 Da wide. To resolve the overlapped mass peaks in this case, we need a much slower scan rate v. This phenomenon can be explained by the bifurcation theory of the non-linear Mathieu equation discussed in Section 2; *i.e.*, when the octopole field is in-phase with the quadrupole field, the ejection is exponential in time; when the octopole field

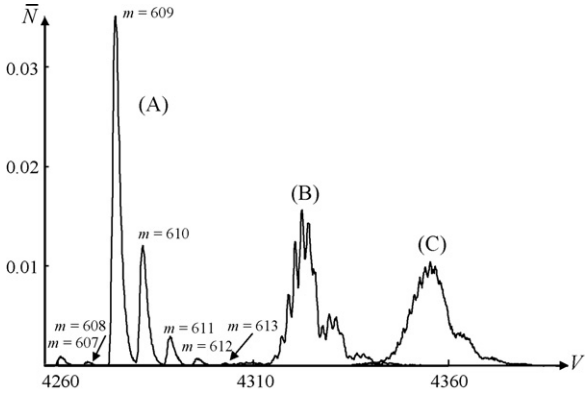

Fig. 5. Simulated mass spectra with 205,900 reserpine ions and $m/e = 607$–613 for three sets of non-pure quadrupole expansion coefficients. Thick line (labeled A): in-phase octopole field with expansion coefficients listed in the second column of Table 1; thin lines: out-of-phase octopole field with same expansion coefficients except that $C_4 = -2C_4^{\mathrm{T}}$ (spectrum B), and $C_4 = -3C_4^{\mathrm{T}}$ (spectrum C). For all the spectra the buffer-gas (helium) pressure is 10^{-3} Torr and temperature is 300 K. The reserpine–helium collision cross-section is estimated to be $\sigma = 167.1$ Å^2. The ordinate $\bar{N}$ is the normalized ion count.

is out-of-phase with the quadrupole field, the ejection follows a square-root law. Therefore, two adjacent mass peaks can be resolved if and only if the ejection time is short compared with the time needed to scan through the two mass peaks.

4. Discussion

The simple bifurcation analysis near the instability threshold provides an analytical prediction for ejection speed. A slight variation in a trap's geometry that creates a small, in-phase octopole field may result in an improvement of mass resolution because the octopole field increases the ejection speed. This method can be extended readily to other non-linear resonance instabilities, such as the $\beta_r + \beta_z = 1$ instability or quasi-periodic excitation, as long as two well-separated scales exist such that one can transform the non-linear equation to a normal form using a perturbation expansion method. This will help engineers to design new traps with higher mass resolution, scan speed and storage stability.

We should also mention earlier work by Sudakov [24] and Makarov [39]. They both studied the inflorescence of a weak octopole on Mathieu equation using the so called *pseudopotential well approximation* [40] and got similar results for slowly varying envelope of the ions' axial displacement. Based on the general non-linear Mathieu equation (10) with $F(z)$ as an arbitrary polynomial, our approach is more general and can be readily extended to study the influence of a single high-order multipole or a superposition of any number of high-order multipoles, as long as their magnitude is small compared to that of the quadrupole.

There are various ways to create a weak, in-phase octopole field. Examples include adding a bump to the exit end-cap, or stretching end-caps from the center of the device by a small distance δ. It should be noted that there exists an optimized value for octopole field amplitude. For a stretched ion trap with geometry shown in Fig. 1, for instance, the optimized octopole field amplitude corresponds to a stretching distance $\delta \approx 1$ mm. This agrees with both numerical and real experiments.

Our hard-sphere scattering model described in Section 2 implies that any ion–buffer-gas interactions are necessarily elastic collisions. Clearly this model does not do justice to the long range molecular interaction. Furthermore, the assumption of elastic collisions implies that no kinetic energy is lost or created in the process. We know that buffer-gas molecules such as helium or hydrogen have numerous excited states and they can act as energy sources or sinks during the collision processes. Therefore, both the trapped ions and the buffer-gas molecules can absorb or emit discrete amounts of energy during transitions from one atomic state to another. However, the assumption of elastic hard-sphere scattering has the advantage of making the collisions readily soluble. In most literatures the buffer-gas effects are modeled as a continuous damping force $\mathbf{f}_{\mathrm{d}} = -\kappa\dot{\mathbf{r}}$ with κ the damping constant. This force would cause all the stable trajectories to damp to the center of the trap as $t \to \infty$. In fact, even a single ion in the presence of damping gas would not relax to a full stop at the center of the trap, because the random bombardment by buffer-gas molecules would continuously excite the ion. Our model at least correctly reflects the fact that there exists a balance between collision focusing and collision excitation, and introduces randomness into the ionic motion.

The use of 2D traps is rapidly becoming important in mass spectrometry [41]. A 2D ion trap has a greater ion trapping efficiency, greater ion capacity before observing space-charging effects, and a faster ion ejection rate than a traditional 3D ion trap (Paul trap) mass spectrometer. This is because for a 3D trap ions need to be confined to a small volume at the center of the trap for optimum performance while for a 3D trap ions can spread out in the axial dimension without degrading the performance. The governing equations for ionic motion in a 2D trap is also the Mathieu equation of the form (1) with $u = y$ or z, or the non-linear Mathieu equation of the form (10) for z when weak, high-order multipoles are taken into account. All our analyses and simulation algorithms can be directly applied to the 2D ion trap.

Ion traps are now purposely designed with non-perfect quadrupole geometry. Significant efforts have been made to improve the mass resolution and correct mass shift caused by higher-order multipole fields. This work opens an easy and quick way to serve these purposes. A systematic numerical investigation can be carried out to determine, *e.g.*, the optimized bumps' size and end-caps' stretching distance, or the parameters in quasi-periodic excitation field. Perhaps one of the most interesting extensions of this work is to develop theory and algorithms for an additional dipole field; investigating quasi-periodic excitation with an rf modulation will also be a challenging task.

Acknowledgements

The author extends his grateful thanks to Dr. Kenneth Newton for his comments and suggestions. The calculation for molecular radii by Dr. Lijie Wang is deeply acknowledged. The author also thanks Dr. Mingda Wang, Dr. August Specht, and Dr. Jean-Louis Excoffier for informative discussions and comments.

References

[1] W. Paul, H. Steinwedel, Z. Naturforsch., Teil A 8 (1953) 448.
[2] P.H. Dawson (Ed.), Quadrupole Mass Spectrometry and its Applications, AIP Press, NY, 1995.
[3] R.E. March, R.J. Hughes, Quadrupole Storage Mass Spectrometry, Wiley, NY, 1989.
[4] R.E. March, J.F.J. Todd (Eds.), Practical Aspects of Ion Trap Mass Spectrometry, vol. I, CRC Press, Boca Raton, 1995.
[5] N.W. McLachlan, Theory and Applications of Mathieu Equations, Clarendon, Oxford, 1947.
[6] M. Abramowitz, I.A. Stegun (Eds.), Handbook of Mathematical Functions, Dover, NY, 1972;
V.A. Yakubovich, V.M. Starzhinskii, Linear Differential Equations with Periodic Coefficients, vols. I, II, Wiley, NY, 1975.
[7] J.P.E. Syka, Commercialization of the Quadrupole Ion Trap (Chapter 4), in Ref. [4].
[8] J.D. Jackson, Classical Electrodynamics, Wiley, NY, 1962.
[9] Y. Wang, J. Franzen, Int. J. Mass Spectrom. Ion Process. 132 (1994) 155.
[10] L. Ding, J. Mass Spectrom. 39 (2004) 471.
[11] B.-N. Jiang, The Least-Squares Finite Element Method, Springer, Berlin, 1998.
[12] L.S. Brown, G. Gabrielse, Rev. Mod. Phys. 58 (1986) 233.
[13] R.S. Zounes, R.H. Rand, Nonlinear Dynam. 27 (2002) 87.
[14] F. Verhulst, Acta Appl. Math. 70 (2002) 231.
[15] M. Cartmell, Introduction to Linear Parametric and Nonlinear Vibrations, Chapman and Hall, London, 1990.
[16] H.W. Broer, M. Levi, Arch. Rat. Mech. Anal. 131 (1995) 225;
H.W. Broer, C. Simo, Bol. Soc. Brasil Mat. 29 (1998) 253;
H.W. Broer, C. Simo, J. Diff. Eqs. 166 (2000) 290.
[17] M. Ruijgrok, A. Tend, F. Verhulst, ZAMM 73 (1993) 255;
M. Ruijgrok, Studies in parametric and autoparametric resonance, Ph.D. Thesis, University of Utrech, 1995;
M. Ruijgrok, F. Verhulst, Prog. Nonlinear Diff. Eqs. Appl. 19 (1996) 279.
[18] V.I. Arnold, Geometrical Methods in the Theory of Ordinary Differential Equations, Springer-Verlag, NY, 1983.
[19] G. Iooss, M. Adelmeyer, Topics in Bifurcation Theory, World Scientific, Singapore, 1992.
[20] J. Guckenheimer, P. Holmes, Nonlinear Oscillations, Dynamical Systems and Bifurcations of Vectorfields, Springer-Verlag, NY, 1983;
J.M.T. Thompson, I. Stewart, Nonlinear Dynamics and Chaos, Wiley, NY, 1986;
Y.A. Kuznetsov, Elements of Applied Bifurcation Theory, 2nd ed., Springer-Verlag, NY, 1998.
[21] F.C. Moon, Chaotic Vibrations: An Introduction for Applied Scientists and Engineers, Wiley, NY, 1987.
[22] S. Wiggins, Global Bifurcation and Chaos, Appl. Math. Sciences, vol. 73, Springer-Verlag, NY, 1988;
S. Wiggins, Introduction to Applied Nonlinear Dynamical Systems and Chaos, Springer-Verlag, NY, 1990.
[23] H.O. Peitgen, H. Jurgens, D. Saupe, Chaos and Fractals, Springer-Verlag, NY, 1996;
F. Verhulst, Nonlinear Differential Equations and Dynamical Systems, Springer-Verlag, NY, 1996.
[24] M. Sudakov, Int. J. Mass Spectrom. 206 (2001) 27.
[25] J.H. Parks, A. Szöke, J. Chem. Phys. 103 (1995) 1422.
[26] A. Gianninas, N. Cowan, Simulating dynamics of thorium ions in a Paul trap at liquid nitrogen temperatures, Research Project (198-459D) Report, Physics Dept., McGill University, 2003.
[27] See, *e.g.*, S.K. Stein, A. Barcellos, Calculus and Analytic Geometry, McGraw-Hill, 1992.
[28] A.D. Becke, J. Chem. Phys. 98 (1993) 5648.
[29] C. Lee, W. Yang, R.G. Parr, Phys. Rev. B 37 (1988) 785.
[30] W.J. Hehre, L. Random, Paul von R. Schleyer, John A. Pople, Ab Initio Molecular Orbital Theory, Wiley, New York, NY, 1986.
[31] See *e.g.*;
J. Foresman, A. Frisch, Exploring Chemistry with Electronic Structure Methods: A Guide to Using Gaussian, 2nd ed., Gaussian, Inc., CT, 1998;
M. Frisch, J. Foresman, A. Frish, Gaussian 03 User's Reference, Gaussian, Inc., CT, 2003;
See also the official Gaussian website http://www.gaussian.com for manuals and product information.
[32] M. García Sucre, G. Urbina-Villalba, L. Lameda, R.E. Parra, Langmuir 13 (1997) 5739.
[33] G. Javahery, B. Thomson, J. Am. Soc. Mass Spectrom. 8 (1997) 697.
[34] S. Wu, Rapid Commun. Mass Spectrom., submitted for publication.
[35] L. Verlet, Phys. Rev. 165 (1967) 201;
K. Hazzard1, J. Wilkins, Rev. Undergraduate Res. 2 (2003) 19.
[36] J.M. Haile, Molecular Dynamics Simulations: Elementary Methods, Wiley, NY, 1992;
D. Frenkel, B. Smit, Understanding Molecular Simulations: From Algorithms to Applications, Academic Press, San Diego, 1996;
D.C. Rapaport, The Art of Molecular Dynamics, 2nd ed., Cambridge University Press, 2004.
[37] T. Schlick, Molecular Modeling and Simulation, Springer-Verlag, NY, 2002.
[38] Deuflhard, J. Hermans, B. Leimkuhler, A.E. Mark, S. Reich, R.D. Skeel (Eds.), Computational Molecular Dynamics: Challenges, Methods, Ideas, Springer-Verlag, Berlin, 1999.
[39] A.A. Makarov, Anal. Chem. 68 (1996) 4257.
[40] R.F. Wuerker, H. Shelton, R.V. Langmuir, J. Appl. Phys. 30 (1959) 342;
F.G. Major, H.G. Dehmelt, Phys. Rev. 170 (1968) 91.
[41] J.C. Schwartz, M.W. Senko, J.E. Syka, J. Am. Soc. Mass Spectrom. 13 (2002) 659;
A.L. Michaud, A.J. Frank, C. Ding, X.Z. Zhao, D.J. Douglas, J. Am. Soc. Mass Spectrom. 16 (2005) 835;
N. Konenkov, F. Londry, C. Ding, D.J. Douglas, J. Am. Soc. Mass Spectrom. 17 (2006) 1063.